Rayleigh-Bénard Convection in Open and Closed Rotating Cavities

Martin P. King
Abdus Salam International Centre for Theoretical Physics, Strada Costiera 11, Trieste, Italy

Michael Wilson

J. Michael Owen
e-mail: ensjmo@bath.ac.uk

Department of Mechanical Engineering, University of Bath, Bath BA2 7AY, UK

Buoyancy effects can be significant in the rotating annular cavities found between compressor discs in gas-turbine engines, where Rayleigh numbers above 10^{12} are common. In some engines, the cavity is "closed" so that the air is confined between four rotating surfaces: two discs and inner and outer cylinders. In most engines, however, the cavity is "open" and there is an axial throughflow of cooling air at the center. For open rotating cavities, a review of the published evidence suggests a Rayleigh–Bénard type of flow structure, in which, at the larger radii, there are pairs of cyclonic and anti-cyclonic vortices. The toroidal circulation created by the axial throughflow is usually restricted to the smaller radii in the cavity. For a closed rotating annulus, solution of the unsteady Navier–Stokes equations, for Rayleigh numbers up to 10^9, show Rayleigh–Bénard convection similar to that found in stationary enclosures. The computed streamlines in the r-θ plane show pairs of cyclonic and anti-cyclonic vortices; but, at the larger Rayleigh numbers, the computed isotherms suggest that the flow in the annulus is thermally mixed. At the higher Rayleigh numbers, the computed instantaneous Nusselt numbers are unsteady and tend to oscillate with time. The computed time-averaged Nusselt numbers are in good agreement with the correlations for Rayleigh–Bénard convection in a stationary enclosure, but they are significantly higher than the published empirical correlations for a closed rotating annulus. [DOI: 10.1115/1.2432898]

Keywords: Rayleigh–Bénard convection, rotating cavities

1 Introduction

Buoyancy-induced flow occurs in the rotating annular cavities found between the compressor disks in gas-turbine engines. In some engines the cavity is *closed*, and the trapped air is confined between four rotating surfaces: two disks and an inner and outer cylindrical surface. In most engines, however, the cavity is *open*, as shown in Fig. 1, and there is an axial throughflow of cooling air in the clearance between the center of the discs and a rotating shaft. (Although the shaft usually rotates at a different angular speed from that of the discs, in this paper it is assumed to have the same speed, Ω.) Figure 2 shows a schematic diagram of the open and closed rotating cavities that are the subject of this paper.

Rayleigh–Bénard convection can occur in the fluid enclosed between two, stationary, horizontal plates, the lower of which is heated. The buoyancy-induced flow structure (see Refs. [1–3]) comprises a parallel array of contrarotating vortices with horizontal axes, as shown in Fig. 3. King and Wilson [4] showed that a similar flow structure can occur in a rotating annulus, where the outer cylindrical surface is heated. In this case, where the centripetal acceleration, $\Omega^2 r$, is much greater than the gravitational acceleration, g, the axes of the counter-rotating vortices in the annulus are in the axial direction. (In an engine, $\Omega^2 r/g$ is typically of the order of 10^4, and Rayleigh numbers are usually greater than 10^{12}.)

This paper considers the occurrence of Rayleigh–Bénard convection, and related buoyancy-induced flow, in both open and closed rotating cavities. Section 2 presents the linear equations for rotating fluids, and Sec. 3 reviews some relevant published work. Section 4 describes the governing equations and computational methods that are used to produce the computed flow structures and Nusselt numbers that are presented in Sec. 5 for a closed cavity. The principal conclusions are summarized in Sec. 6.

2 Linear Equations for Rotating Fluids

Consider a frame of reference, rotating with angular speed Ω about an axis located at point 0. In cylindrical-polar coordinates, u, v, and w are the components of velocity in the r, θ, z directions.

The so-called linear equations are a simplified form of the Navier–Stokes equations when the nonlinear inertial terms are negligibly small compared with the Coriolis acceleration. Strictly, the linear equations are only valid when $|u|$ and $|v|$ are much smaller than Ωr. There are, however, many flows where the equations give good predictions of experimental measurements even when $|u|$ and $|v|$ are of similar magnitude to Ωr (see Refs. [5,6]). The equations developed below are based on those derived by Farthing et al. [7]; they are used here to show their relevance to Rayleigh–Bénard flow.

For steady flow, the continuity equation and the inviscid linear equations (which, in meteorology, are referred to as the *geostrophic equations*) can be expressed as

$$\partial_r(\rho r u) + \partial_\theta(\rho v) + \partial_z(\rho r w) = 0 \tag{1}$$

$$2\Omega v = \frac{1}{\rho}\partial_r p - \Omega^2 r \tag{2a}$$

$$2\Omega u = -\frac{1}{\rho r}\partial_\theta p \tag{2b}$$

$$0 = \frac{1}{\rho}\partial_z p \tag{2c}$$

Equations (1) and (2) lead to the result that

Contributed by the Internal Gas Turbine Institute (IGTI) of ASME for publication in the Journal of Engineering For Gas Turbines and Power. Manuscript received October 31, 2005; final manuscript received November 15, 2005. Review conducted by Dilip R. Ballal. Paper presented at the ASME Turbo Expo 2005: Land, Sea and Air (GT2005), Reno, Nevada, June 6–9, 2005, Paper No. GT2005-68948.

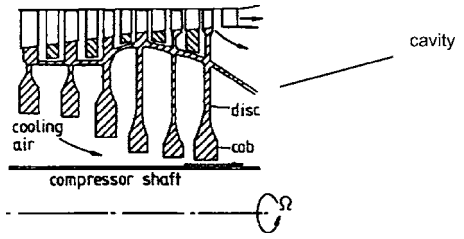

Fig. 1 Simplified diagram of high-pressure compressor rotor with axial throughflow

$$\partial_z(\rho w) = \frac{\Omega}{2}\partial_\theta \rho \tag{3}$$

For incompressible or axisymmetric flow (where $\partial_\theta \rho$ is zero) it follows that ρw is invariant with z. This result, often referred to as the Taylor–Proudman theorem, means that u and v are also invariant with z. Two important consequences should be noted: (i) rotation tends to create two-dimensional (2D) stratified flow, reducing circulation; (ii) radial flow can only occur if $\partial_\theta p \neq 0$. (As shown in Ref. [6], for source-sink flow in a rotating cavity, radial flow is confined to Ekman layers on the discs and there is virtually no flow in the inviscid core of fluid between these layers.)

For incompressible flow, equation (2*a*) can be written as

$$2\Omega v = \frac{1}{\rho}\partial_r P \tag{4}$$

where P is the so-called *reduced pressure* defined by

$$P = p - \frac{1}{2}\rho\Omega^2 r^2 \tag{5}$$

For cyclonic circulation, where $v > 0$, the pressure increases radially. As the pressure at the center of the circulation is lower than that at the outside, cyclonic circulation is associated with low pressure (as in the earth's atmosphere); conversely, anti-cyclonic circulation is associated with high pressure.

In a rotating cavity, Rayleigh–Bénard convection is always associated with an *even* number of vortices; in a stationary enclosure, the number may be odd or even. These cyclonic and anti-cyclonic pairs of vortices create the circumferential pressure gradient that is needed to produce the radial convection of fluid in the rotating cavity. The above results apply to inviscid flow: viscosity tends to reduce the circulation, and heat transfer to the cylindrical surfaces of a rotating cavity occurs in the boundary layers on these surfaces.

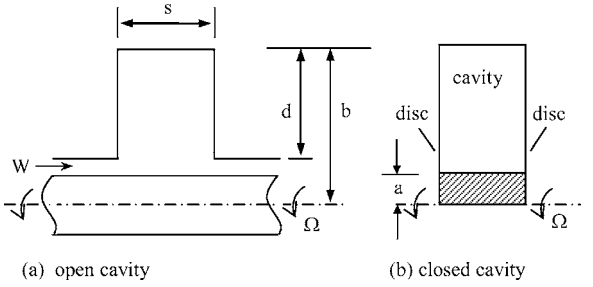

Fig. 2 Schematic diagram of open and closed rotating cavities

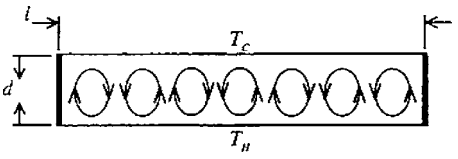

Fig. 3 Rayleigh–Bénard convection in a horizontal stationary enclosure

3 Review of Previous Work

The definition of symbols is given in the Nomenclature.

3.1 Open Rotating Cavities. The Sussex Group [7–12] made measurements and computations for a rotating cavity with an axial throughflow of cooling air for $a/b \approx 0.1$. There was no central shaft, and either the discs or the shroud (the outer cylindrical surface) were heated.

Farthing et al. [7] carried out flow visualization and laser-Doppler anemometry (LDA) studies in both isothermal and heated cavities. For the isothermal case, the axial throughflow was seen to generate a powerful toroidal vortex, in cavities with large gap ratios ($G > 0.4$), the strength of which decreased as the rotational speed increased. Depending on the values of G and Ro, the Rossby number, axisymmetric and nonaxisymmetric vortex breakdown [13] was observed in the central jet. When one or both of the disks were heated, the flow in the cavity became nonaxisymmetric, and cyclonic and anti-cyclonic circulation was observed. The core of fluid between the discs precessed at an angular speed (Ω_c say) slightly less than that of the discs. The ratio of Ω_c/Ω decreased as the temperature difference between the discs and the cooling air increased.

For the case of $G = 0.138$, with both discs heated to the same (radially increasing) temperature, Farthing et al. [8] correlated the Nusselt number, Nu_1, by

$$\mathrm{Nu}_1 = 0.0054\,\mathrm{Re}_z \mathrm{Gr}_1^{0.25} \tag{6}$$

The correlations for natural convection [14] from a heated vertical plate in air (where the centripetal acceleration $\Omega^2 r$ in the definition of Gr_1 is replaced by the gravitational acceleration g, and $(b-r)$ is replaced by the vertical height) are

$$\mathrm{Nu}_1 = 0.36\,\mathrm{Gr}_1^{0.25} \quad \text{for laminar flow} \tag{7a}$$

$$\mathrm{Nu}_1 = 0.022\,\mathrm{Gr}_1^{0.4} \quad \text{for turbulent flow} \tag{7b}$$

For the vertical plate, transition from laminar to turbulent flow occurs at $\mathrm{Gr}_1 \approx 10^9$. For the rotating cavity, Farthing et al. found no evidence of transition even for $\mathrm{Gr}_1 > 10^{11}$, which suggested that the flow might be laminar even at very large values of the Grashof number.

As part of a major European research project [internal cooling air systems in gas turbines (ICAS-GT)] Owen and Powell [15] made measurements in an open cavity, where $a/b = 0.4$ and $G = 0.2$, in which one of the discs was heated. LDA and heat transfer measurements were made for $1.4 \times 10^3 < \mathrm{Re}_z < 5 \times 10^4$ and $4 \times 10^5 < \mathrm{Re}_\phi < 3.2 \times 10^6$. Spectral analysis of the LDA measurements revealed a multi-cell structure comprising one, two or three pairs of vortices. As found in the experiments of Farthing et al., the core of fluid between the discs precessed at an angular speed, Ω_c, less than that of the discs, and Ω_c/Ω decreased as the temperature of the heated disk increased. At the smaller values of Re_z, the measured Nusselt numbers were consistent with buoyancy-induced flow; at the larger values of Re_z, the effect of the axial throughflow became dominant.

Complementary computational research, conducted as part of ICAS-GT, was reported by Smout et al. [16]. Three-dimensional, unsteady, turbulent computations for the open rotating cavity at low values of Re_z produced a multi-cell structure and the computed Nusselt numbers were consistent with the measurements made by Owen and Powell.

Tian et al. [17] computed the flow and heat transfer in a rotating cavity based on the geometry of Farthing et al. Their 3D, steady, turbulent computations showed that the flow structure comprised two parts: Rayleigh–Bénard convection at the larger radii, and forced convection in the central region. The computations suggested that there is a critical Rayleigh number above which the

flow becomes unstable and time dependent.

Johnson et al. [18] investigated the stability characteristics of variable-density swirling flow in rotating cavities. Using a narrow-gap approximation for inviscid flow, they produced criteria for the necessary and sufficient conditions for stability. When the rotating surfaces are colder than the "cooling air" (such as at takeoff in an aeroengine) the flow is stably stratified: the axial throughflow cannot penetrate very far into the cavity and the resulting convective heat transfer is relatively low. Conversely, when the rotating surfaces are hotter than the air (at cruise and landing), the flow is unstable, the axial flow can readily enter the cavity, and the heat transfer is increased as a consequence. (For these unstable conditions, flow visualization revealed "multi-lobe secondary flows" rotating inside the cavities of a compressor drum.)

3.2 Closed Rotating Cavities. The Aachen group [19–22] made measurements and computations for a sealed annulus where the heat flow could be either axial (from a hot disk to a cold one) or radial (from a hot outer cylindrical surface to a cold inner one). The subscripts 2 and 3 are used below for axial and radial heat transfer, respectively. In both cases, the Nusselt numbers represent the ratio of (axial or radial) convection to conduction in the annulus. The Nusselt numbers are spatially and time averaged values.

For $G=0.5$, $a/b=0.52$, $2\times10^8<\mathrm{Ra}_2<5\times10^{10}$, the Nusselt number for the axial case was correlated by

$$\mathrm{Nu}_2 = 0.346\,\mathrm{Ra}_2^{0.124} \tag{8}$$

For the radial case, three different geometries were tested for $10^7<\mathrm{Ra}_3<10^{12}$, and the correlations are given below.

Geometry A (axisymmetric annulus with $G=0.34$, $a/b=0.35$)

$$\mathrm{Nu}_{3,A} = 0.266\,\mathrm{Ra}_3^{0.228} \tag{9a}$$

Geometry B (axisymmetric annulus with $G=0.5$, $a/b=0.52$)

$$\mathrm{Nu}_{3,B} = 0.317\,\mathrm{Ra}_3^{0.211} \tag{9b}$$

Geometry C (annulus with 45 deg segments with $G=0.5$, $a/b=0.52$)

$$\mathrm{Nu}_{3,C} = 0.365\,\mathrm{Ra}_3^{0.213} \tag{9c}$$

From the definitions of Ra_3 and Re_3 it follows that

$$\mathrm{Ra}_3 = (s/r_m)\mathrm{Pr}\,\beta\Delta T\,\mathrm{Re}_3^2 \tag{10}$$

where

$$\mathrm{Re}_3 = \Omega r_m s/\nu \tag{11}$$

Therefore the Rayleigh number depends on both the rotational Reynolds number, Re_3, and the buoyancy parameter, $\beta\Delta T$. Coriolis forces increase as Ω increases, and the results of Sec. 2 suggest that circulation inside the annulus should be reduced as Ω, and hence Re_3, increases. In the experiments, for a given value of Ra_3, $\mathrm{Re}_{3,B}$ was greater than $\mathrm{Re}_{3,A}$. Consequently, $\mathrm{Nu}_{3,B}<\mathrm{Nu}_{3,A}$, although the differences were relatively small.

As shown in Sec. 2, radial flow can only occur in the inviscid core of fluid if $\partial_\theta p\neq0$. For annuli A and B, this pressure gradient is created by pairs of cyclonic and anti-cyclonic vortices. In annulus C, the radial walls in the cavity allow a pressure gradient to exist without the need for vortex pairs. Bohn et al. [20] found that, in annulus C, there was anti-cyclonic circulation, with an isothermal core, in each of the eight segments. This circulation provided enhanced convection so that, for a given value of Ra_3, the Nusselt numbers in annulus C were slightly greater than those in either A or B.

For Rayleigh–Bénard convection in stationary, horizontal enclosures, King [23] used dimensional and physical arguments to show that $\mathrm{Nu}_3=A_1\mathrm{Ra}^{a1}+A_2\mathrm{Ra}^{a2}+\ldots$, where A_1, A_2, a_1, and a_2 are constants. Niemela et al. [24] correlated Nu_3 for low and high Rayleigh numbers, and Grossman and Lohse [3] produced the semi-empirical result

$$\mathrm{Nu}_3 = 0.27\,\mathrm{Ra}^{1/4} + 0.038\mathrm{Ra}^{1/3} \tag{12}$$

Holland et al. [25] obtained the correlation, for $\mathrm{Pr}=0.7$

$$\mathrm{Nu}_3 = 1 + 1.44\,\max\{1-1708/\mathrm{Ra},0\} + \max\{(\mathrm{Ra}/5830)^{1/3}-1,0\} \tag{13}$$

King and Wilson [4] solved the unsteady 2D laminar equations (see Sec. 4) for an annulus (with the outer surface heated) in which the gravitational acceleration, g, was replaced by a *constant* centripetal acceleration ($\Omega^2 b$). Their computed streamlines showed the vortex structure associated with Rayleigh–Bénard convection. The computed Nusselt numbers, for $10^4<\mathrm{Ra}<10^9$ and $a/b=0.5$ and 0.7, were in good agreement with the above correlations for a stationary enclosure.

4 Governing Equations and Computational Methods

The unsteady Navier–Stokes equations are expressed, using dimensionless variables, in vorticity-streamfunction and velocity–vorticity formulations for the 2D and 3D computations, respectively. Derivations, from the original primitive-variables forms of the equations using Boussinesq approximations and suitable substitutions, are given by Lewis [26] and King [23].

The 2D dimensionless equations in cylindrical polar coordinates and in a rotating frame of reference for radial–tangential (r-θ) flow in streamfunction-vorticity form are

$$\bar{\omega} = \nabla^2\bar{\psi} \tag{14}$$

$$\frac{1}{\mathrm{Pr}}\left[\partial_{\bar{t}}\bar{\omega} + \frac{1}{\bar{r}}J(\bar{\omega},\bar{\psi})\right] + \frac{2\mathrm{Ra}_\phi}{\bar{r}\mathrm{Re}_\phi\mathrm{Pr}}J(\bar{T},\bar{\psi}) + \mathrm{Ra}_\phi\partial_\theta\bar{T} = \nabla^2\bar{\omega} \tag{15}$$

$$\partial_{\bar{t}}\bar{T} + \frac{1}{\bar{r}}J(\bar{T},\bar{\psi}) = \nabla^2\bar{T} \tag{16}$$

where the Jacobian operator is given by $J(A,B)=\partial_{\bar{r}}A\,\partial_\theta B - \partial_{\bar{r}}B\,\partial_\theta A$ and $\bar{t},\bar{T},\bar{\omega}$, and $\bar{\psi}$ are the nondimensional time (or Fourier number), temperature, vorticity and streamfunction, respectively.

The vorticity-velocity formulation for the dimensionless 3D equations are

$$\frac{1}{\mathrm{Pr}}\left[\partial_{\bar{t}}A + (\underline{\bar{u}}\,.\,\nabla)A - A\partial_{\bar{r}}\bar{u} - \frac{B}{\bar{r}}\partial_\theta\bar{u} - C\partial_{\bar{z}}\bar{u}\right]$$

$$- 2\mathrm{Re}_\phi\partial_{\bar{z}}\bar{u} + \frac{2\mathrm{Ra}_\phi}{\mathrm{Re}_\phi\mathrm{Pr}}(\bar{T}\partial_{\bar{z}}\bar{u} + \bar{u}\partial_{\bar{z}}\bar{T})$$

$$= \nabla^2 A - \frac{2}{\bar{r}^2}\partial_\theta B - \frac{A}{\bar{r}^2} \tag{17}$$

$$\frac{1}{\mathrm{Pr}}\left[\partial_{\bar{t}}B + (\underline{\bar{u}}\,.\,\nabla)B - A\left(\partial_{\bar{r}}\bar{v} - \frac{\bar{v}}{\bar{r}}\right) - \frac{B}{\bar{r}}(\bar{u} + \partial_\theta\bar{v}) - C\partial_{\bar{z}}\bar{v}\right]$$

$$- 2\mathrm{Re}_\phi\partial_{\bar{z}}\bar{v} + \frac{2\mathrm{Ra}_\phi}{\mathrm{Re}_\phi\mathrm{Pr}}(\bar{T}\partial_{\bar{z}}\bar{v} + \bar{v}\partial_{\bar{z}}\bar{T})$$

$$+ \bar{r}\mathrm{Ra}_\phi\partial_{\bar{z}}\bar{T} = \nabla^2 B + \frac{2}{\bar{r}^2}\partial_\theta A - \frac{B}{\bar{r}^2} \tag{18}$$

$$\frac{1}{\mathrm{Pr}}\left[\partial_{\bar{t}}C + (\underline{\bar{u}}\,.\,\nabla)C - A\partial_{\bar{r}}\bar{w} - \frac{B}{\bar{r}}\partial_\theta\bar{w} - C\partial_{\bar{z}}\bar{w}\right]$$

$$- 2\mathrm{Re}_\phi\partial_{\bar{z}}\bar{w} + \frac{2\mathrm{Ra}_\phi}{\mathrm{Re}_\phi\mathrm{Pr}}\left(\bar{T}\partial_{\bar{z}}\bar{w} - \bar{u}\partial_{\bar{r}}\bar{T} - \frac{\bar{v}}{\bar{r}}\partial_\theta\bar{T}\right)$$

$$-Ra_{\phi}\partial_{\theta}\bar{T} = \nabla^2 C \tag{19}$$

where A, B, and C are the components of vorticity and $\bar{u}, \bar{v}, \bar{w}$ the nondimensional velocities in the r, θ, and z directions, respectively. The Poisson equations for velocity are derived using the curl of the vorticity and the continuity equation. The velocity expressed in terms of vorticity is then given by

$$\nabla^2 \bar{w} = \frac{1}{\bar{r}}\partial_{\theta}A - \partial_{\bar{r}}B - \frac{B}{\bar{r}} \tag{20}$$

$$\nabla^2 \bar{v} + \frac{2}{\bar{r}}\partial_{\bar{r}}\bar{v} + \frac{\bar{v}}{\bar{r}^2} = \partial_{\bar{r}}C + \frac{2C}{\bar{r}} - \partial_{\bar{z}}A \tag{21}$$

$$\nabla^2 \bar{u} + \frac{2}{\bar{r}}\partial_{\bar{r}}\bar{u} + \frac{\bar{u}}{\bar{r}^2} = \partial_{\bar{z}}B = \frac{1}{\bar{r}}\partial_{\theta}C - \frac{1}{\bar{r}}\partial_{\theta}C - \frac{2}{\bar{r}}\partial_{\bar{z}}\bar{w} \tag{22}$$

The energy equation is

$$\partial_{\bar{t}}\bar{T} + (\bar{u}\,.\,\nabla)\bar{T} = \nabla^2 \bar{T} \tag{23}$$

The boundary conditions for the various dimensionless variables are such that there are no-slip velocity conditions, adiabatic side discs, $\bar{T}=1$ on the outer cylinder, and $\bar{T}=0$ on the inner cylinder. The computations were started from solid-body rotation and a conduction profile in temperature; the unstable flows develop through either numerical rounding errors or an imposed artificial disturbance.

The equations were solved using second-order-accurate finite-difference approximations in space on collocated uniform curvilinear grids for the 2D equations and on staggered grids for the 3D equations. The Arakawa [27] formulation was used to treat the nonlinear terms in the 2D equations. Time-stepping was based on the Du- Fort–Frankel method where values of a dependent variable at the present time step were exchanged for averages of new and previous time-step values. Equations (14) and (20)–(22) are boundary value problems within each time step. To accelerate convergence, they were solved using a V-cycling multigrid routine, incorporating a Gauss–Seidel line relaxation scheme.

The computed Nusselt numbers were based on the ratio of radial convection, at $\bar{r}=1$, to 1D radial conduction in the annulus. The local Nusselt number, Nu_3, was therefore defined as

$$\mathrm{Nu}_3 = \ln(b/a)(\partial_{\bar{r}}\bar{T})_{\bar{r}=1} \tag{24}$$

and the global, or spatially averaged, Nusselt number, $\mathrm{Nu}_{3,\mathrm{av}}$, was obtained by integrating Nu_3 over the area of the outer cylindrical surface.

Various grid and time-step resolutions were used to ensure numerical stability. For the 2D computations, the finest grid resolution was 96×192 (in r-θ) and the smallest time step was 2×10^{-8}; for the 3D computations, they were $32\times32\times128$ (in r-z-θ) and 5×10^{-8}, respectively.

5 Computed Flow in Closed Cavities

5.1 Flow Structure. The results discussed below were obtained by solving the equations given in Sec. 4 for $\mathrm{Pr}=0.7$ and $a/b=0.5$. Limitations in available computing power meant that computations were not practical for Rayleigh numbers greater than 10^9 for 2D flow and 10^6 for 3D flow.

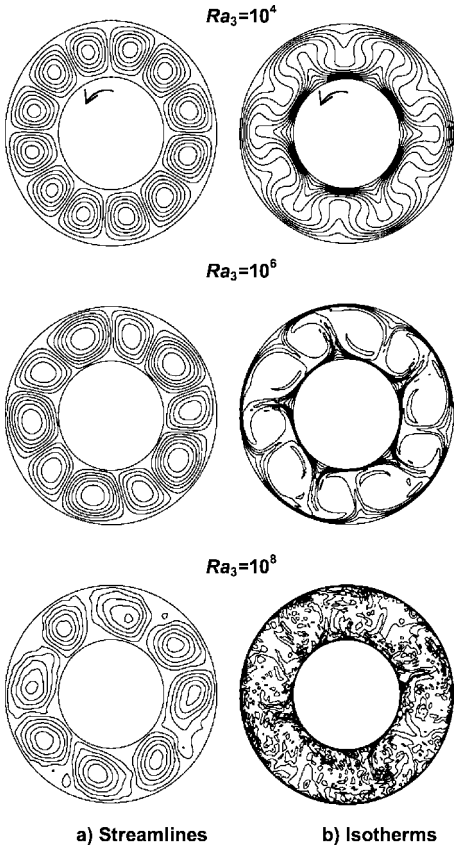

Fig. 4 Computed 2D streamlines and isotherms for $a/b=0.5$

The values of $\beta\Delta T$ used in the computations were chosen to match those in the experiments of Bohn et al. It was assumed that $\beta\Delta T = 1.1\mathrm{Ra}_3^{-0.114}$; as $\mathrm{Ra}_3 \propto \beta\Delta T\,\mathrm{Re}_3^2$, $\beta\Delta T$ varied between 0.44 and 0.1, and Re_3 between 128 and 1.5×10^5 for the range of Rayleigh numbers used in the computations. (As shown in Sec. 2, increasing Ω—and hence increasing Re_3—tends to reduce the circulation in the annulus. As found in the Aachen experiments, for a given value of Ra_3, increasing Re_3 tends to reduce the Nusselt number.)

Figure 4 shows the 2D computations of the instantaneous streamlines and isotherms; the values of $\bar{t}$ are given in Table 1. Although the streamlines show clear evidence of Rayleigh–Bénard convection, the isotherms show a more complicated picture. For $\mathrm{Ra}_3=10^4$, the isotherms show a series of lobes; for $\mathrm{Ra}_3=10^6$, the vortex pairs are clearly visible and their cores appear to be virtually isothermal; for $\mathrm{Ra}_3=10^8$, despite the vortex flow seen in the streamlines, the isotherms suggest that thermal mixing has occurred. Reasons for this mixing are discussed below.

Two-dimensional computations were conducted for $10^{3.5} \le \mathrm{Ra}_3 \le 10^9$, and Table 1 shows the number of pairs of vortices, n, that were observed for each value of Ra_3. The fact that n can vary from 4 to 6 in what appears to be a random fashion suggests that

Table 1 Number of pairs of observable vortices, n, in annulus for $a/b=0.5$

Ra_3	$10^{3.5}$	10^4	$10^{4.5}$	10^5	$10^{5.5}$	10^6	$10^{6.5}$	10^7	$10^{7.5}$	10^8	$10^{8.5}$	10^9
$\bar{t}$	2.5	0.25	0.25	0.2	0.2	0.15	0.04	0.015	0.003	0.01	0.003	0.0015
n(streamlines)	5	6	5	6	5	5	5	5	5	4	6	5
n(isotherms)	5	6	5	6	5	5	5	5	5	—	—	—

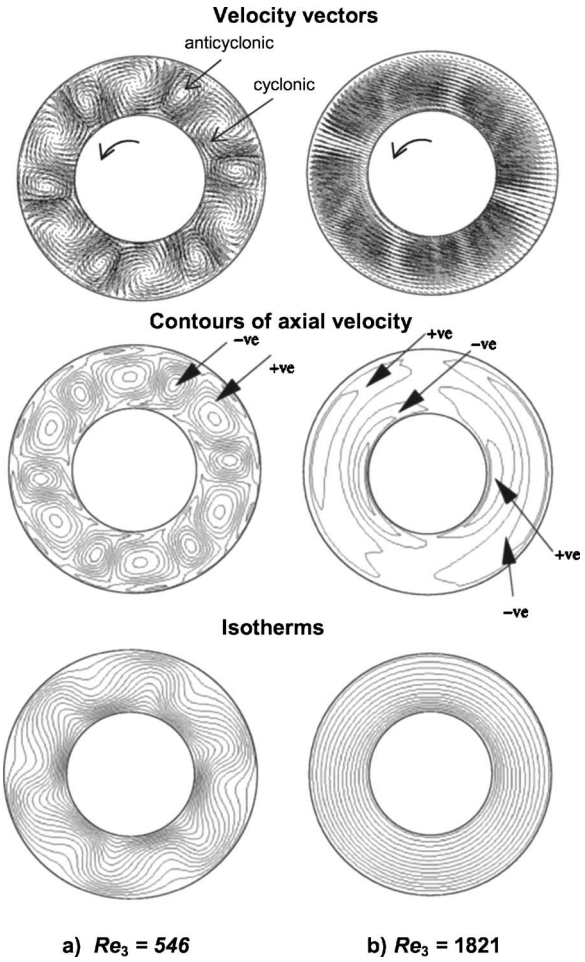

Fig. 5 Computed 3D flow structure at $\bar{z}=0.25$ and for $Ra_3=10^{3.9}$, $a/b=0.5$, $G=0.5$

n is time dependent. (The computations of Lewis [26] for a rotating annulus also showed that the number of vortex pairs could change with time.) The flow *vacillates*, and it is this vacillation that is thought to be responsible for the lack of coherence in the isotherms for $Ra_3 \geq 10^8$: the constantly changing flow structure acts as an effective thermal-mixing device. (*Vacillation* is used to mean an unsteadiness in the flow structure; this includes *structural vacillation* in which the number of vortices can change with time.)

The phenomenon of coherent flow structures and thermal mixing was also seen, above a critical Rayleigh number, in computations in a stationary annulus [23]. The measurements of Niemela et al. [24] for Rayleigh–Bénard flow in a stationary enclosure confirmed that large-scale coherent flow structures with thermal mixing could occur for Rayleigh numbers up to 10^{17}. This suggests that the phenomenon is physical.

Figure 5 shows the 3D computations of the instantaneous flow structure in an annulus with a gap ratio of $G=0.5$ for $Ra_3=10^{3.9}$ and $Re_3=546$ and 1821. For $Re_3=546$, the velocity vectors, at $z/s=0.25$ in the r-θ plane, show a similar structure to the 2D computations for $Ra_3=10^4$ in Fig. 4.

In the 3D computations for $Re_3=546$, the contours of axial velocity show that there is axial flow away from the discs (+ve) in the cyclonic (low pressure) vortices, and flow towards the disc (−ve) in the anti-cyclonic vortices. (This can be seen more clearly in the results for $Re_3=546$ than for $Re_3=1821$.) The isotherms show a lobe-type of structure similar to that shown in the 2D computations in Fig. 4.

For $Re_3=1821$, the 3D flow structure in Fig. 5 is far less clear but, for the reason stated above, increasing Re_3 reduces the circulation, and the circular isotherms show that conduction dominates over convection.

5.2 Nusselt Numbers. Figure 6 shows the computed variation of $Nu_{3,av}$, the global Nusselt number, with time $\bar{t}$ for $Ra_3=10^4$, 10^6, and 10^8. For stably stratified flow, where only conduction occurs, $Nu_{3,av}=1$, which is the case as $\bar{t}\rightarrow 0$. For $Ra_3=10^4$, the flow becomes unstable (that is, Rayleigh–Bénard convection occurs) for $\bar{t}>0.1$, and $Nu_{3,av}$ increases to a constant value of approximately 2.5. For $Ra_3=10^6$, however, $Nu_{3,av}$ never achieves a steady value: for $\bar{t}>0.1$, periodic oscillations occur and $7<Nu_{3,av}<9$. For $Ra_3=10^8$, the oscillations are aperiodic, and $30<Nu_{3,av}<40$. The oscillations in $Nu_{3,av}$ are attributed to the vacillating flow structure discussed above.

Figure 7 shows the variation of $\overline{Nu}_{3,av}$, the computed time-average global Nusselt number, with Ra_3. The computed Nusselt numbers are in good agreement with the correlations for a stationary enclosure but differ significantly from those for a rotating annulus.

King [23] conducted 3D laminar computations, for $Ra_3 \leq 10^6$, and the computed Nusselt numbers were in good agreement with the correlations for a stationary enclosure. Limitations in computing power meant that it was not possible to compute $\overline{Nu}_{3,av}$ at values of Ra_3 high enough to make comparisons with the empirical correlations for the rotating annulus. It is possible that 3D computations, with an appropriate turbulence model, could produce better agreement with the correlations for the rotating annulus, but that is beyond the scope of this paper. (It should be noted that Sun et al. [28] achieved good agreement with the results of Bohn et al. using a 3D compressible time-accurate code with a low-Mach-number preconditioner.)

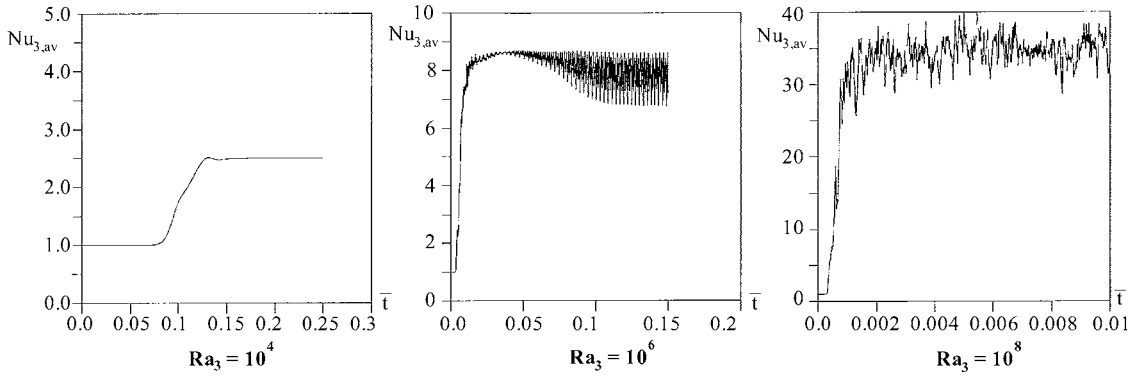

Fig. 6 2D computations of variation of $Nu_{3,av}$ with $\bar{t}$ for $a/b=0.5$

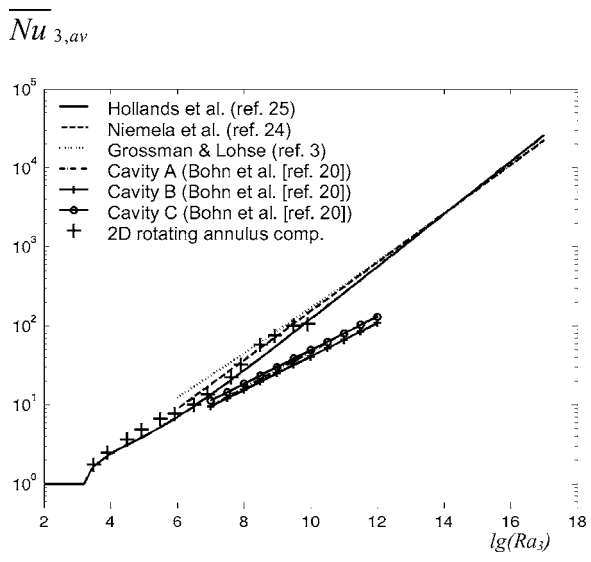

Fig. 7 2D computations of variation of $\overline{Nu}_{3,av}$ with Ra_3 for $a/b=0.5$

Heating the disks, or the outer surfaces, of a rotating cavity can produce buoyancy-induced flow. For the case of an open rotating cavity with an axial throughflow of cooling air, previously published work shows that a complex flow structure occurs: cyclonic and anti-cyclonic vortex pairs are created at large radii and the toroidal circulation induced by the throughflow is confined to the smaller radii.

For a closed rotating cavity (or sealed annulus), where the outer cylindrical surface is hotter than the inner one, the computed flow structure is similar to the Rayleigh–Bénard convection that occurs in stationary horizontal enclosures. Two-dimensional unsteady solutions of the Navier–Stokes equations, for rotational Rayleigh numbers up to 10^9 in a cavity with $a/b=0.5$, show that cyclonic and anti-cyclonic vortex pairs are created in the r-θ plane. For large Rayleigh numbers, the computed streamlines show clear evidence of vortex pairs, whereas the thermal contours suggest that the flow in the annulus is thermally mixed. This result, which has also been observed in stationary enclosures, is thought to be caused by vacillation in the flow structure.

The computed instantaneous Nusselt numbers also show unsteady behavior at the higher Rayleigh numbers. The time-averaged Nusselt numbers are in good agreement with the correlations for Rayleigh–Bénard convection in stationary enclosures, but they are significantly higher than the empirical correlations for a closed rotating annulus. The reason for this overprediction is not understood, but it is possible that the use of an appropriate turbulence model may produce better agreement between the computations and measurements for the rotating annulus.

Acknowledgment

The authors wish to thank Sarah Fuge for typing this paper, and we thank the reviewers for their constructive comments.

Nomenclature

a,b = inner, outer radius of cavity
A,B,C = components of vorticity in r, θ, z directions
d = vertical height of stationary enclosure; radial height of annulus
g = gravitational acceleration
G = s/b, gap ratio
Gr_1 = $\Omega^2 r(b-r)^3\beta\Delta T/\upsilon^2$, Grashof number for open cavity
k = thermal conductivity
l = horizontal length of stationary enclosure
L = characteristic length
$\dot{m}$ = mass flow rate
n = number of vortex pairs
Nu_1 = $q(b-r)/k\Delta T$, Nusselt number for open cavity
$\mathrm{Nu}_{2,av}$ = $q_{av}s/k\Delta T$, average Nusselt number for annulus (axial heat flow)
Nu_3 = q/q_{cond}, local Nusselt number for annulus (radial heat flow) or stationary enclosure
$\underline{\mathrm{Nu}}_{3,av}$ = global-average of Nu_3
$\overline{\mathrm{Nu}}_{3,av}$ = time average of $\mathrm{Nu}_{3,av}$
Pr = ν/α, Prandtl number
q = heat flux
r = radius
$\bar{r}$ = r/b, nondimensional radius
r_m = $\frac{1}{2}(a+b)$, mean radius of annulus
Ra = $gd^3\beta\Delta T/\upsilon\alpha$, Rayleigh number for stationary enclosure
Ra_2 = $\Omega^2 r_m s^3\beta\Delta T/\nu\alpha$, Rayleigh number for annulus (axial heat flow)
Ra_3 = $\Omega^2 r_m d^3\beta\Delta T/\upsilon\alpha$, Rayleigh number for annulus (radial heat flow)
Ra_ϕ = $\Omega^2 b^4\beta\Delta T/\nu\alpha$, rotational Rayleigh number
Re_3 = $\Omega r_m s/\upsilon$, rotational Reynolds number for annulus
Re_z = WL/ν, axial Reynolds number
Re_ϕ = $\Omega b^2/\nu$, rotational Reynolds number
Ro = $W/\Omega a$, Rossby number
s = axial gap between disks
t = time
$\bar{t}$ = $\alpha t/b^2$, nondimensional time (Fourier number)
T = absolute temperature
$\bar{T}$ = $(T-T_c)/(T_H-T_c)$, nondimensional temperature
u,v,w = radial, tangential and axial components of velocity in a rotating frame of reference
$\bar{u},\bar{v},\bar{w}$ = values of u,v,w normalized with respect to Ωb
W = bulk-average axial velocity
z = axial distance from left-hand disk
$\bar{z}$ = z/s, nondimensional axial distance
α = thermal diffusivity
β = T_{ref}^{-1}, volume expansion coefficient
ΔT = (T_H-T_c) temperature difference
μ = dynamic viscosity
ν = kinematic viscosity
ρ = density
Ω = angular speed of cavity
Ω_c = angular speed of fluid core
ω = vorticity
$\bar{\omega}$ = $\omega b^2/\alpha$, nondimensional vorticity
ψ = streamfunction in r-θ plane
$\bar{\psi}$ = ψ/α nondimensional streamfunction

Subscripts

av = average value
C = cold surface
cond = conduction
H = hot surface
I = inlet value
ref = reference value

References

[1] Koschmieder, E. L., 1993, *Bénard Cells and Taylor Vortices*, Cambridge University Press, Cambridge, UK.
[2] Siggia, E. D., 1994, "High Rayleigh Number Convection," Annu. Rev. Fluid Mech., **26**, pp. 137–168.
[3] Grossman, S., and Lohse, D., 2000, "Scaling in Thermal Convection: A Uni-

fying Theory," J. Fluid Mech., **407**, pp. 27–56.
[4] King, M. P., and Wilson, M., 2002, "Free Convective Heat Transfer Within Rotating Annuli," *Proceedings 12th International Heat Transfer Conference*, Vol. 2, Grenoble, France, pp. 465–470.
[5] Owen, J. M., and Rogers, R. H., 1989, "Flow and Heat Transfer in Rotating-Disc Systems," *Rotor-Stator Systems*, Vol. 1, Research Studies Press, Taunton, UK.
[6] Owen, J. M., and Rogers, R. H., 1995, "Flow and Heat Transfer in Rotating-disc Systems," *Rotating Cavities*, Vol. 2, Research Studies Press, Taunton, UK.
[7] Farthing, P. R., Long, C. A., Owen, J. M., and Pincombe, J. R., 1992, "Rotating Cavity With Axial Throughflow of Cooling Air: Flow Structure," J. Turbomach., **114**, pp. 237–246.
[8] Farthing, P. R., Long, C. A., Owen, J. M., and Pincombe, J. R., 1992, "Rotating Cavity With Axial Throughflow of Cooling Air: Heat Transfer," J. Turbomach., **114**, pp. 229–236.
[9] Long, C. A., 1994, "Disk Heat Transfer in a Rotating Cavity With an Axial Throughflow of Cooling Air," Int. J. Heat Fluid Flow, **15**, pp. 307–316.
[10] Long, C. A., and Tucker, P. G., 1994, "Shroud Heat Transfer Measurements From a Rotating Cavity With an Axial Throughflow of Air," J. Turbomach., **116**, pp. 525–534.
[11] Long, C. A., and Tucker, P. G., 1994, "Numerical Computation of Laminar Flow in a Heated Rotating Cavity With an Axial Throughflow of Air," Int. J. Numer. Methods Heat Fluid Flow, **4**, pp. 347–365.
[12] Long, C. A., Morse, A. P., and Tucker, P. G., 1997, "Measurement and Computation of Heat Transfer in High Pressure Compressor Drum Geometries With Axial Throughflow," J. Turbomach., **119**, pp. 51–60.
[13] Owen, J. M., and Pincombe, J. R., 1979, "Vortex breakdown in a rotating cylindrical cavity," J. Fluid Mech., **90**, pp. 109–127.
[14] Jaluria, Y., 1980, "Natural Convection Heat and Mass Transfer," Pergamon, London.
[15] Owen, J. M., and Powell, J., 2004, "Buoyancy-Induced Flow in a Heated Rotating Cavity," ASME J. Eng. Gas Turbines Power, **128**, pp. 128–134.
[16] Smout, P. D., Chew, J. W., and Childs, P. R. N., 2002, "ICAS-GT: A European Collaborative Research Programme on Internal Cooling Air Systems for Gas Turbines," ASME Paper No. GT-2002-30479.
[17] Tian, S., Tao, Z., Ding, S., and Xu, G., 2004, "Investigation of Flow and Heat Transfer in a Rotating Cavity With Axial Throughflow of Cooling Air," ASME Paper No. GT2004-53525.
[18] Johnson, B. V., Lin, J. D., Daniels, W. A., and Paolillo, R., 2004, "Flow Characteristics and Stability Analysis of Variable-Density Rotating Flows in Compressor-Disk Cavities," ASME Paper No. GT2004-54279.
[19] Bohn, D., Dibelius, G. H., Deuker, E., and Emunds, R., 1994, "Flow Pattern and Heat Transfer in a Closed Rotating Annulus," J. Turbomach., **116**, pp. 542–547.
[20] Bohn, D., Deuker, E., Emunds, R., and Gorzelitz, V., 1995, "Experimental and Theoretical Investigations of Heat Transfer in Closed Gas Filled Rotating Annuli," J. Turbomach., **117**, pp. 175–183.
[21] Bohn, D., Edmunds, R., Gorzelitz, V., and Kruger, U., 1996, "Experimental and Theoretical Investigations of Heat Transfer in Closed Gas-Filled Rotating Annuli II," J. Turbomach., **118**, pp. 11–19.
[22] Bohn, D., and Gier, J., 1998, "The Effect of Turbulence on the Heat Transfer in Closed Gas-Filled Rotating Annuli," J. Turbomach., **120**, pp. 824–830.
[23] King, M. P., 2003. "Convective Heat Transfer in a Rotating Annulus," Ph.D. thesis, University of Bath, Bath, UK.
[24] Niemela, J. J., Skrbek, L., Sreenivasan, K. R., and Donnelly, R. J., 2000, "Turbulent Convection at Very High Rayleigh Numbers," Nature (London), **404**, pp. 837–840.
[25] Hollands, K. G. T., Raithby, G. D., and Konicek, L., 1975, "Correlation Equations for Free Convection Heat Transfer in Horizontal Layers of Air and Water," Int. J. Heat Mass Transfer, **18**, pp. 879–884.
[26] Lewis, T., 1999, "Numerical Simulation of Buoyancy-Induced Flow in a Sealed Rotating Cavity," Ph.D. thesis, University Bath, Bath, UK.
[27] Arakawa, A., 1996, "Computational Design for Long-Term Numerical Integration of the Equations of Fluid Motion: Two-Dimensional Incompressible Flow. Part 1," Comput. Phys., **1**, pp. 119–143.
[28] Sun, X., Kifoil, A., Chew, J. W., and Hills, N. J., 2004, "Numerical Simulation of Natural Convection in Stationary and Rotating Cavities," ASME Paper No. GT2004-53528.